

Surface acoustic wave based pumping in a microchannel

Tao Wang¹ · Qi Ni¹ · Nathan Crane¹ · Rasim Guldiken¹

Received: 17 November 2015 / Accepted: 10 February 2016 / Published online: 27 February 2016
© Springer-Verlag Berlin Heidelberg 2016

Abstract Pumping and manipulation of liquids in microfluidic channels are important for many mechanical, chemical and biomedical applications. Surface acoustic wave based devices fabricated on high-efficiency piezoelectric substrates have been recently investigated for mixing and separation application within microfluidic channels. In this paper, we introduce a novel integrated surface acoustic wave based pump for liquid delivery and precise manipulation within a microchannel. The device employs a hydrophobic surface coating (Cytop) in the device design to decrease the friction force and increase the bonding. Contrary to previous surface acoustic wave based pumps which were mostly based on the filling and sucking process, we demonstrate long distance media delivery (up to 8 mm) and high pumping velocity increasing the device's application space and mass production potential. Additionally, the device design does not need precise layers of water and glass between substrate and channel, simplifying the design significantly. In this study, we conducted extensive parametric studies to quantify the effects of the liquid volume pumped, microchannel size, input applied power as well as the existence of hydrophobic surface coating on the pumping velocity and pump performance. Our results indicate that the pumping velocity for a constant liquid volume with the same applied input power can be increased by over 130 % (2.31 vs 0.99 mm/min) by employing a hydrophobic surface coating (Cytop) in a thinner microchannel (250 vs 500 μm) design. This device can be used in circulation,

dosing, metering and drug delivery applications which necessitates small-scale precise liquid control and delivery.

1 Introduction

Pumping, mixing and separation in microfluidic systems are actively investigated due to increased demand for low-cost and portable devices for biomedical, chemical and mechanical applications. For mixing (Jo and Guldiken 2013; Tan et al. 2009; Sriharan et al. 2006) and separation (Dung Luong and Trung Nguyen 2010; Guldiken et al. 2012a; Jo and Guldiken 2012, 2014) purposes, many fairly high-efficiency devices have been thoroughly investigated. Pumps are one of the key components for delivering and controlling flow in microfluidic systems. Typically, liquids are difficult to pump in microchannels due to low Reynolds number which is well below 10. At low Reynolds numbers, friction forces dominate the pumping forces and liquid appears to be more viscous than it is, resulting in large flow resistances and laminar flow profile (Kockmann 2006). Currently, the most widely used pumping types in microfluidic systems are mechanical and electrical pumps (Shabani and Cho 2011; Laser and Santiago 2004). However, mechanical pumps need high power and electrical pumps need high voltage for efficient operation. Surface acoustic wave (SAW) based droplet manipulation at free surface has been reported with high velocity up to several centimeters per second (Alghane et al. 2011). However, only efficient droplet pumping on free surfaces, not within a microfluidic channel, was reported. As compared to alternatives, liquid manipulation and pumping with SAW is a non-contact technique capable of precise and highly repeatable flow manipulation. Also, SAW pumps do not require high power or voltage for high-efficiency operation.

✉ Rasim Guldiken
guldiken@usf.edu

¹ Department of Mechanical Engineering, University of South Florida, Tampa, FL 33620, USA

Previous studies reported that SAWs can only push liquids in a closed microchannel for a very short distance (1.1 mm) which is essentially a filling process from outside the channel with very low filling speed at the SAW propagation direction. However, microfluidic applications necessitate not just forcing liquid into a microchannel with only few nanoliters to hundred nanoliters liquid volume (Cecchini et al. 2008; Masini et al. 2010) but precise fluid manipulation within a microchannel (Girardo et al. 2008). There has been a recent surface wave driven pump that accomplished continuous liquid pumping inside a polydimethylsiloxane (PDMS) closed channel (Schmid et al. 2012). However, this device needs water and glass layers in the design between substrate and channel. The existence of precisely controlled water and glass layers limits the reliability, repeatability and mass production potential. In this paper, we introduce a novel integrated surface acoustic wave based liquid delivery and precise manipulation within a microchannel which is not a filling or sucking process. We demonstrate high speed, large volume delivery and manipulation from a long distance with low sample media loss. PDMS is widely used as biocompatible material with advantages of low reflection effect on SAW propagation, wide temperature range and high optical transparency (Jo and Guldiken 2014). The device employs a hydrophobic surface coating (Cytop) on the microchannel for decreasing the friction force and increasing the bonding. When compared to other closed channel micropumps reported, this device can precisely manipulate a liquid inside a microchannel in a long distance up to 8 mm without requiring high power input.

2 Device operation, simulation and design

Figure 1 illustrates conceptual view of the surface acoustic wave based fluid manipulation and pumping investigated

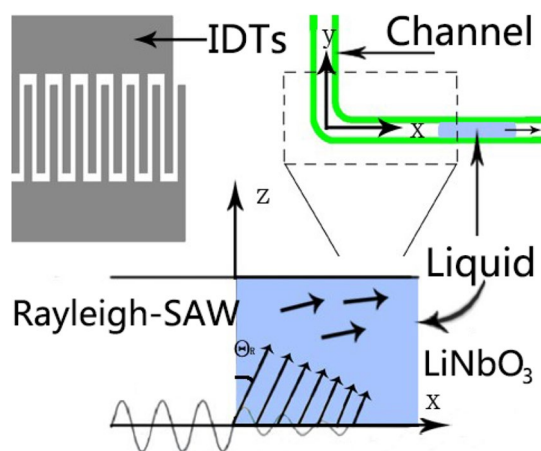


Fig. 1 Conceptual view of the liquid pumping and manipulation induced by surface acoustic waves

in this study. After surface waves are generated by judiciously designed interdigital transducers (IDTs), the waves propagate towards the microchannel from the IDTs and interact with the liquid located in the channel. The compressional component of the wave is diffracted at the Rayleigh angle into the fluid. When the surface acoustic waves travel through the substrate, the temperature increases as the applied voltage is increased (Tseng et al. 2006). Hence, the IDTs transfer the heat to the air and liquid inside the microchannel. As the temperature of the air and water is increased due to wave propagation, the saturation pressure of water vapor will increase. This will cause increase in the evaporation rate, pushing the liquid forward. Therefore the force that causes fluid manipulation in the channel is the resultant force of the body force and expansion force that moves the liquid with low power consumption.

$$\frac{dN_e}{dt} = A_e \alpha_v \frac{1}{\sqrt{2\pi m k T}} (P_e - P) \quad (1)$$

$$\rho_w = \frac{P_e}{RT} M \quad (2)$$

From the Hertz-Knudsen formula (Eq. 1) (Rahimi and Ward 2005) which is expressed as the absolute rates of the evaporation at the liquid and vapor interface, the evaporation rate can be estimated with temperature (T is temperature of the liquid) and vapor pressure (P_e and P are the equilibrium vapor pressure and ambient hydrostatic pressure, respectively). In Eq. (1), m is the mass of the liquid, k is the Boltzmann constant, α_v is the sticking coefficient and A_e is the evaporating surface of area. In majority of the applications, the evaporation rate is small and the expansion force is negligible. However, when the temperature of the liquid is increased from room temperature (22 °C) to 38 °C due to propagating acoustic wave, the evaporation rate for liquid can be estimated as $1.353 \times 10^{-5} \mu\text{l/s}$ ($1.353 \times 10^{-11} \text{ kg/s}$). Note that this calculation was performed for a microchannel with a 500 μm width and 70 μm height and 0.22 μl media volume. The density of the water vapor can also be estimated (Eq. 2) (Feder 1992). From the evaporation rate and vapor density, the volumetric vapor generation rate can be obtained as 0.01 $\mu\text{l/s}$. As compared to the small liquid volume of 0.22 μl , vapor generation rate will cause a significant expansion force on the liquid.

Finite element simulations (FEM) was conducted as a part of this study to optimize the design parameters by using the commercial COMSOL Multiphysics 4.4 software (Mohan et al. 2013; Kaletta and Wenger 2014). As illustrated in Fig. 2, we simulated only a single wavelength portion of the entire SAW device to simplify the geometry and reduce the computing power. In the simulations, the structure and electric potential boundaries (Γ_L and Γ_R as indicated

Fig. 2 **a** SAW transducer geometry employed in the simulations; **b** profile of the IDT fingers formed by 100 nm chromium deposited on a 500 μm 127.8° Lithium Niobate substrate

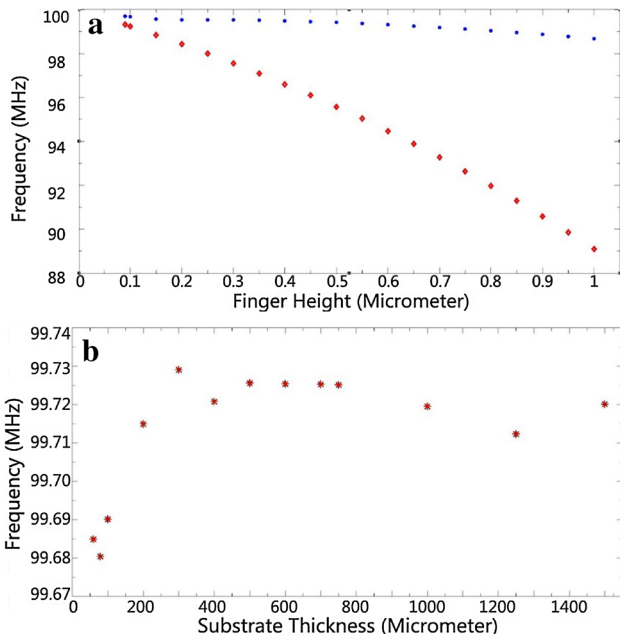
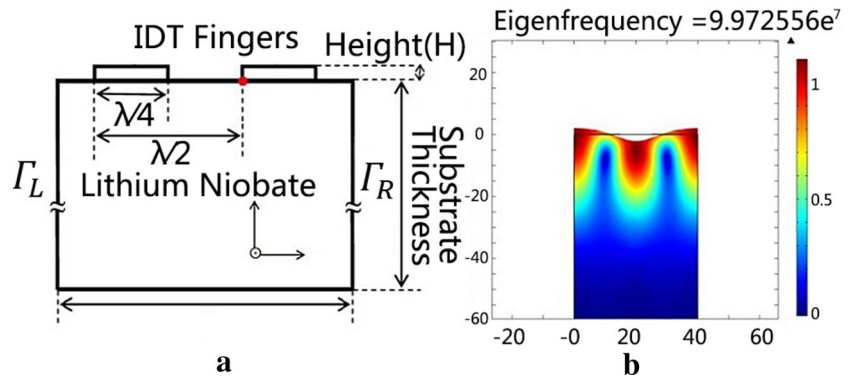


Fig. 3 **a** Simulated operation frequency as a function of the IDT finger height and material selection; **b** simulated operation frequency as a function of the substrate thickness

Table 1 Device parameters used for the design and fabrication of the IDT transducers

Wavelength (λ)	40 μm	Channel width 1	500 μm
Finger width	10 μm	Channel width 2	250 μm
Finger pitch	40 μm	Channel height	70 μm
Number of fingers	50 pairs	Operation frequency	97.75 MHz

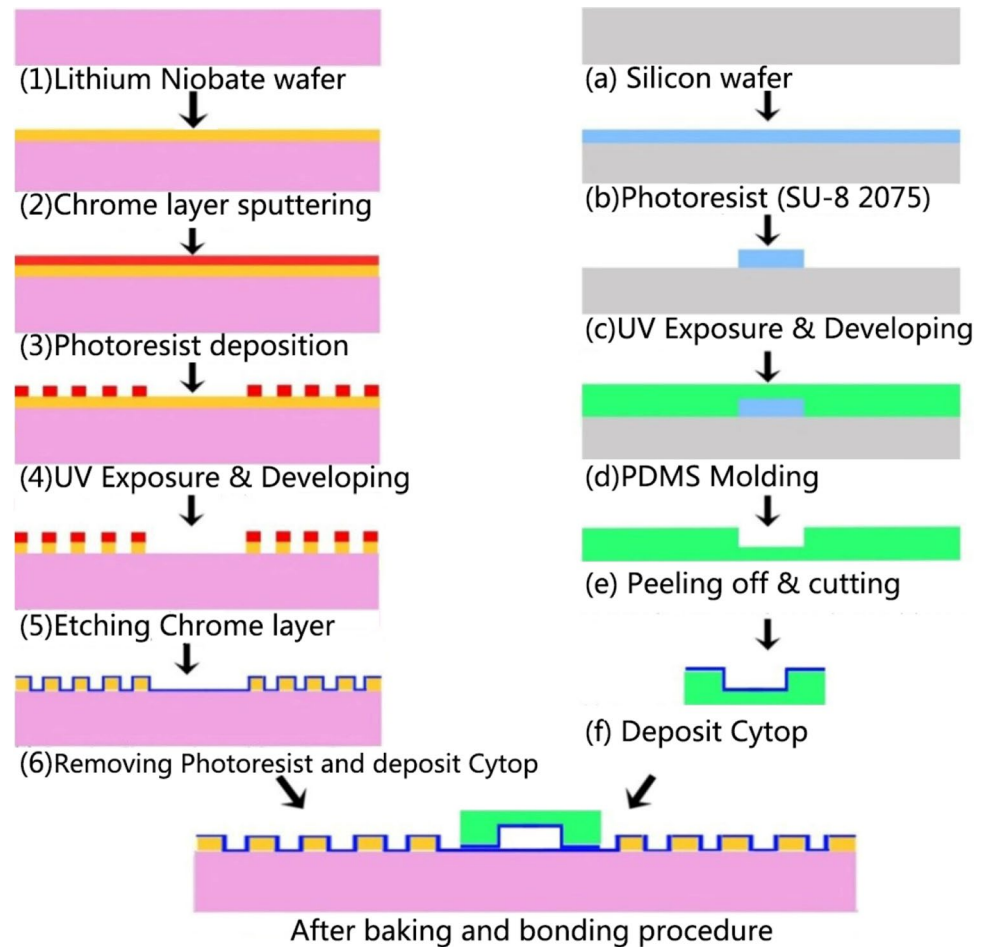
in Fig. 2a) was set as periodic in nature to simulate multiple pairs of IDT fingers with a simplified geometry. This model will allow us to investigate the SAW velocity as a function of the IDT finger thickness and its material. We investigated the effect of the gold and chromium finger heights ranging from 90 nm to 1 μm on the transducer frequency response.

An optimized layer thickness and materials will result in operation frequency closer to the design frequency.

First group of simulations was conducted by employing the eigenfrequency module of the COMSOL to obtain the effect of different heights and materials on the design frequency (Fig. 3a). For a constant substrate thickness of 500 μm and wavelength (λ as indicated in Fig. 2a) of 40 μm , the theoretical design resonance frequency turns out to be 99.75 MHz ($f = V_{\text{Saw}}/\lambda$). It should be highlighted that the effects of finger height and substrate thickness are not captured in this theoretical resonance frequency calculations that is employed by many researchers. However, as can be clearly observed from the Fig. 3a, the operation frequency of the device is a function of the IDT finger height. In fact, if one employs Gold (Au) with Chromium (Cr) as the adhesion layer, the operation frequency is a significant function of the finger height. For instance, if one uses a 0.5 μm thick finger in the design, the actual operation frequency is shifted to 95.5 MHz from 99.75 MHz. Employing Chromium as the IDT finger material results in far less variation in the operation frequency for the entire range of finger heights investigated in this study. Second group of simulations were conducted to investigate the effect of substrate thickness on the operation frequency of the SAW devices (Fig. 3b). One can observe from this figure that the effect of substrate thickness on the device operation frequency is minimal. In fact, this is an important result in that many of the wafer substrate manufacturers do not specify the exact wafer thickness but rather substrate thickness range (such as 500–550 μm). Hence even with the existence of this variation, the operation frequency stays almost constant. It should be highlighted that this simulations were conducted for 100 MHz operation frequency, for applications requiring high frequency operation (such as in the GHz range), the effect of substrate thickness may in fact become more significant. Based on these simulation studies, we employed 100 nm chromium IDT finger material patterned on a \sim 500 μm Lithium Niobate substrate.

Table 1 illustrates the final design parameters of the IDTs used in this study. The wavelength, width and pitch of the

Fig. 4 Fabrication process flow for SAW transducers, PDMS molding, Cytop layer spinning and bonding. All steps were completed in the cleanroom facilities of the University of South Florida



IDT fingers, and aperture were designed as 40, 10, 40, and 5 mm, respectively. Two different channel widths were used: 500 and 250 μm . The channel height was kept constant at 70 μm . Different channel widths were investigated to quantify the effect of the liquid velocity. The transducer operation (resonant) frequency was obtained by the ratio of the velocity of the propagating wave to the wavelength (λ); $f = V_{\text{SAW}}/\lambda$.

3 Transducer fabrication and microchannel integration

The surface acoustic wave pump was fabricated in four steps: patterning of interdigital transducers (IDTs) on a lithium niobate wafer, PDMS microchannel fabrication, Cytop layer coating, and the bonding of PDMS microfluidic channel to the lithium niobate wafer housing the IDTs (Guldiken et al. 2012). Figure 4 illustrates the fabrication process flow of the SAW pumping device. For forming the IDTs, Y-cut X-propagation lithium niobate wafer (128°LiNbO_3 , Universitywafer, MA, USA) was used. After rinsing the Lithium Niobate substrate with acetone, methanol and DI water; a 100 nm chrome was deposited by using the CRC sputtering

system. Then, a 1.6 μm -thick photoresist layer (S1813, Shipley, Marlborough, MA, USA) was spun on the Lithium Niobate substrate. After exposure and developing, the chrome was etched by the chrome etchant (CR-7S, Cyantek, Fremont, CA, USA). IDT fabrication was then completed after the final step of photoresist stripping.

The microchannel was fabricated by PDMS micro molding technique. After the channel mold is formed, PDMS (Sylgard™ 184 kit Dow Corning, Midland, MI, USA) is poured onto the SU-8 mold. Bonding of the IDT substrate and microchannel as well as the Cytop layer deposition was conducted after the fabrication of IDTs and microchannel separately. The PDMS channel was treated with oxygen plasma first; then both the IDT substrate and the PDMS channel was coated with Cytop® 809 M (ASAHI GLASS Co. Ltd, Japan) via spin coating with the average thickness of 1.8 μm on the substrate. After separately pre-baking in an oven at 100 $^\circ\text{C}$, a gauge needle was used to create the inlets and outlets. The Cytop layer was annealed at 160 $^\circ\text{C}$ for an hour as a final step (Uchida 2003). Finally, the PDMS and the substrate were bonded and uniform pressure was applied. The fabricated IDTs and channel feature on the substrate is illustrated in Fig. 5.

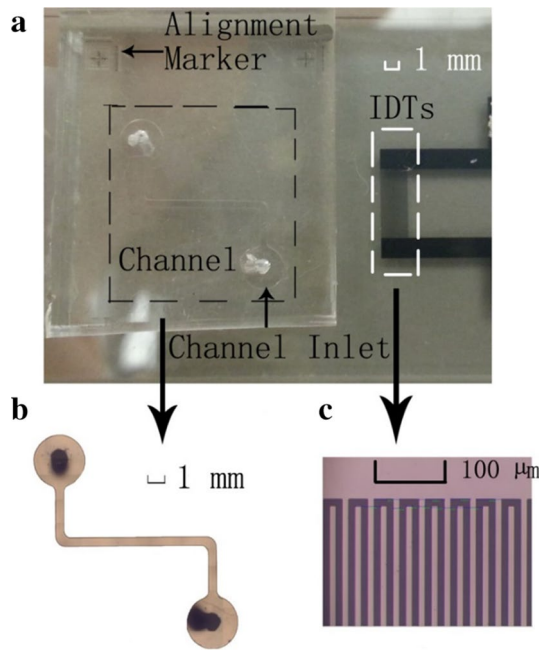


Fig. 5 **a** Aligned IDTs and microchannel on the substrate; **b** the closeup of the microchannel design investigated in this study; **c** the details of the chrome IDTs

4 Experimental setup

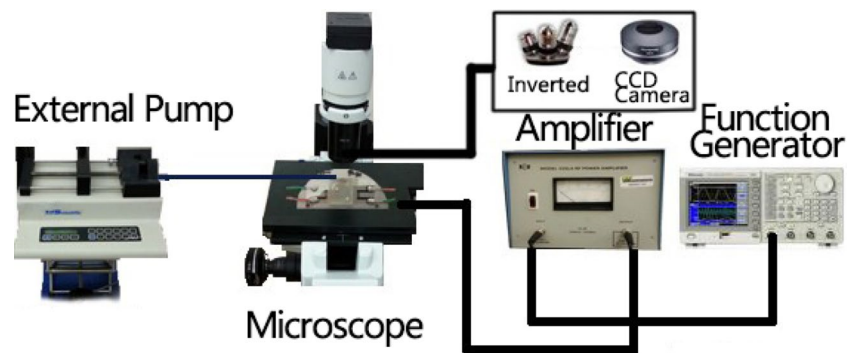
An inverted microscope (IX-51, Olympus) with a CCD camera was used to visualize and record the experimental data collected (Fig. 6). De-ionized water was injected into the channel from the inlet by an external syringe pump (KDS200, KD Scientific, Holliston, MA, USA). RF power amplifier (325LA, ENI) was used to amplify an AC signals generated by a function generator (AFG3022B, Tektronix). Displacement inside the microchannel was recorded by a CCD camera at 21 fps with a resolution of 1376×1038 .

As the input power is related to the amplitude of the surface acoustic wave which determines the pumping velocity (Alghane et al. 2012), a wide-range of applied input power

values (ranging from 0 to 7.5 W) was investigated to obtain the velocity dependence on input power. Also, in order to investigate the effect of liquid volume on the pumping velocity, two different representative volumes (0.22 and 0.11 μL) were used. Additionally, channel width with 250 and 500 μm were used to investigate the effect of channel width on pumping velocity.

Before delving into a detailed parametric study, we investigated the effect of the most common microfluidic channel material choice, PDMS, on the pumping. The contact angle of water on PDMS, which is hydrophobic, is around 110° for static drops (Mata et al. 2005). However, fluid tends to stick to the PDMS surface due to the high contact angle hysteresis. The conventional syringe pump method was used to show the large adhesion force between the fluid and the PDMS surface after plasma bonding. First, a droplet ($\sim 2 \mu\text{L}$) of de-ionized (DI) water was placed onto the substrate, then a needle was inserted into the droplet. A programmable syringe pump was connected to the other end of the needle and fluid was added to the droplet at a flow rate of $5 \mu\text{L}/\text{min}$. After 3 min, the pumping direction was reversed and fluids was withdrawn from the droplet. The shape of the droplet was captured using a digital camera during the infusion/withdrawing of the fluid and the image was processed using ImageJ software. The contact angle of the droplet during the infusion and withdrawing phase is defined as the advancing angle and the receding angle, respectively. In Fig. 7, a large difference between the advancing and receding contact angles was observed which was also observed in prior studies (Cordeiro et al. 2009). The difference between the two angles is commonly known as contact angle hysteresis which can cause a strong adhesion force that will prevent the motion of the fluid or droplet. To prevent this, a $1 \mu\text{m}$ layer of Cytop coating was introduced to both the PDMS channel and the lithium niobate substrate. Static contact angle significantly increased by the Cytop layer as shown in the Fig. 7e, f and contact angle hysteresis decreased from 35° to 10° . The only drawback of the existence of hydrophobic layer in the design was that the insertion loss of the IDTs increased by around 2 dB.

Fig. 6 Experimental setup: An external pump was connected to the channel inlet to pump the liquid into the channel. Function generator generated a continuous sine wave to the amplifier which is connected to the IDTs. Inverted Microscope with CCD camera was used to visualize and record the liquid pumping



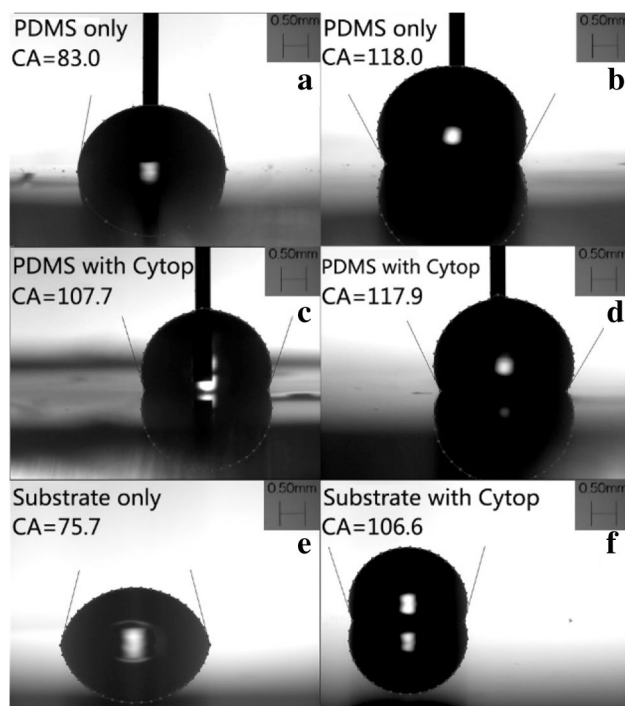


Fig. 7 **a** The receding contact angle of the drop on the PDMS surface without Cytop layer; **b** the advancing contact angle of the drop on the PDMS surface without Cytop layer; **c** the receding contact angle of the drop on the PDMS surface with Cytop layer; **d** the advancing contact angle of the drop on the PDMS surface with Cytop layer; **e** the static contact angle of the drop on the lithium niobate substrate surface without Cytop layer; **f** the static contact angle of the drop on the substrate with Cytop layer

5 Results and discussion

The liquid pumping was accomplished in this study with IDTs placed 5–8 mm away from the microchannel sidewalls. Initial experiments were conducted with both inlet and outlet open (Fig. 8). Figure 9 illustrates the pumping experiment in the 250 μm sealed channel without Cytop layer in the device design over 75 s. The power applied for this case was 6.5 W and liquid volume was 0.11 μl . After the SAWs were excited with continuous sine wave, the liquid initially started to eject droplets at the low power condition (commonly referred as atomization) as illustrated in Fig. 9. As the input power was increased, the ejected droplet diameter started increasing (Murochi et al. 2007). At around 3 W of input power, in addition to atomization, the liquid started to move and at 6 W of input power, the atomization stopped while the liquid was being pumped.

Additional sets of experiments were conducted by sealing the inlet of the microchannel with an off-the-shelf masking tape as illustrated in Fig. 8. The applied input power ranged from 2 to 6.5 W and two types of surface coating were used (Lithium Niobate substrate without any coating

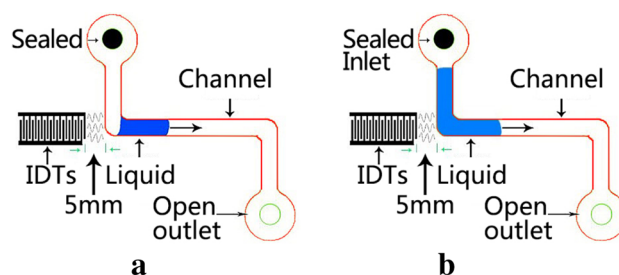


Fig. 8 An illustration of different volume of liquid pumping in the channel with sealed inlet and open outlet. Liquid volume in **a**, **b** are 0.11 and 0.22 μl , respectively

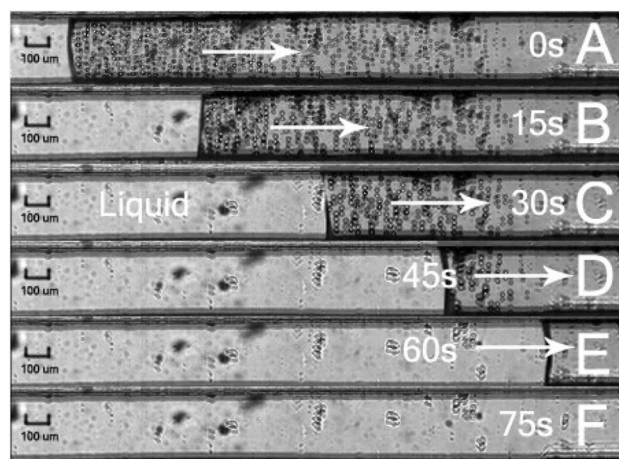


Fig. 9 The pumping experiment in the 250 μm channel without Cytop over 75 s. The power is 6.5 watts and liquid volume is 0.11 μl . Due to the limitation of the field of view of the microscope, only partial channel is shown

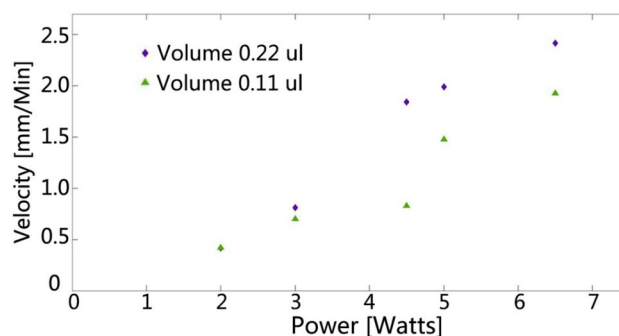


Fig. 10 Experimental pumping velocity as a function of applied input power with two different liquid volumes (0.22 and 0.11 μl) in a 500 μm microchannel with the Cytop layer coating in the design

and Lithium Niobate substrate and channel walls coated with Cytop). Increasing the input power causes increased acoustic wave amplitude. This led to higher acoustic body force as well as evaporation rate. As a result, the pumping force

was composed of both acoustic body force and an expansion force. Increasing the input power resulted in higher heat generation further increasing the total pumping force. Hence, the applied input power was found to be proportional to the pumping velocity. Figure 10 illustrates the pumping velocity as a function of applied input power with two different liquid volumes in a 500 μm microchannel with the Cytop layer in the design. Increasing the input applied power resulted in increasing the pumping velocity for both liquid volume cases investigated. One can observe from individual experimental data points that for applied input power range from 2 to 3 w, the pumping velocities were not a strong function of the volume of the liquid being pumped. Note that this power range corresponds to pumping of the liquid sample with atomization present. However, the larger liquid volume case (0.22 μl) resulted in larger pumping velocity as compared to the lower liquid volume case (0.11 μl) once the power is increased further. Higher pumping velocity is obtained with higher liquid volume case for the same power input because the liquid in the higher volume case is exposed to larger body force in the direction of wave propagating. As can be observed from Fig. 8, larger volume case also has smaller inlet spatial available for expansion pushing the liquid in the desired direction.

Also, extensive experiments were conducted to investigate the effect of the coating of the microchannel surfaces on pumping velocity. Figure 11 illustrates the experimentally obtained pumping velocity as a function of applied input power for a 500 μm microchannel with/without the Cytop layer in the design for two different liquid volumes: 0.22 μl (Fig. 11a) and 0.11 μl (Fig. 11b). Additionally, Fig. 12 shows the experimentally obtained pumping velocity as a function of applied input power for a thinner (250 μm) microchannel with/without the Cytop layer in the design for two different liquid volumes: 0.11 μl (Fig. 12a) and 0.054 μl (Fig. 12b). Increasing the input applied power resulted in increasing the pumping velocity for all microchannel width and liquid volume cases investigated. One can observe from both Figs. 11 and 12 that for the same liquid volume and input power applied cases, hydrophobic surface coating (Cytop) increases the pumping velocity for both microchannel widths and liquid volumes investigated. When one compares Fig. 11b to Fig. 12a, the effect of hydrophobic surface coating on the pumping velocity for the same liquid volume for different microchannel widths can be observed. At the low input power cases (2–3 W), there was no significant effect of hydrophobic coating on the pumping velocity due to increased (2 dB) insertion loss with the Cytop layer in the design. However at the larger power consumption cases (>3 W), the inclusion of hydrophobic coating in the channel design has an increased effect on the pumping velocity for wider microchannel (500 μm) as compared to thinner channel width (250 μm). The reason for obtaining higher

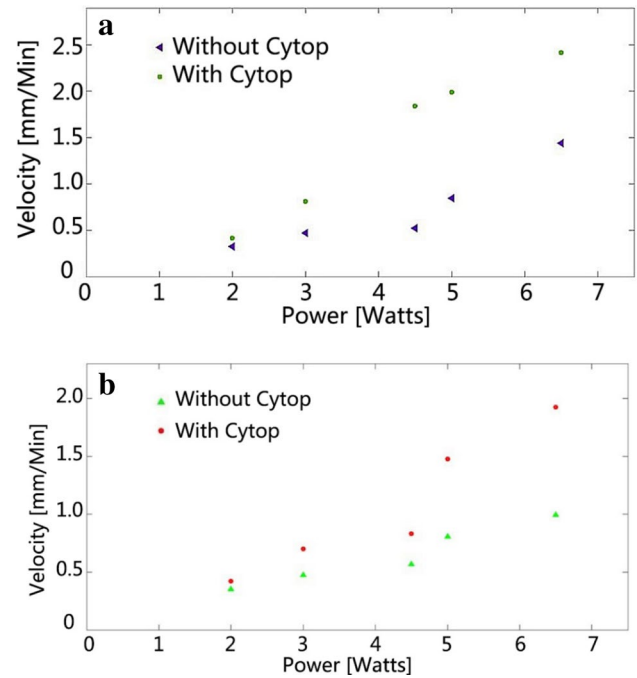


Fig. 11 Experimental pumping velocity as a function of applied input power in a 500 μm microchannel with/without the Cytop layer in the design for two different liquid volumes: 0.22 μl (a) and 0.11 μl (b)

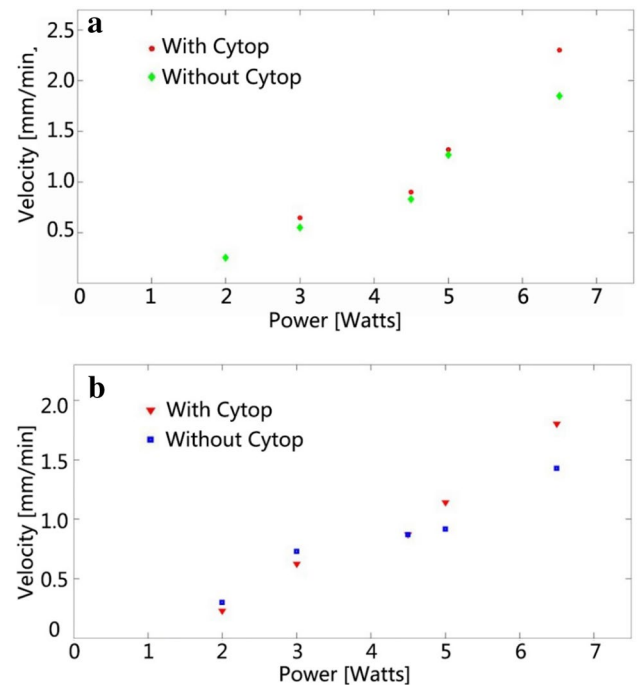


Fig. 12 Experimental pumping velocity as a function of applied input power in a 250 μm microchannel with/without the Cytop layer in the design for two different liquid volumes: 0.11 μl (a) and 0.054 μl (b)

pumping velocity for thinner microchannel as opposed to wider channel with the same liquid volume is that the length of the fluid within the microchannel is longer for the thinner microchannel resulting in increased resultant force in the longitudinal direction (along the length of the microchannel) causing higher pumping velocity.

6 Conclusions

In this study, we conducted a thorough investigation of liquid pumping within a microfluidic channel by using the phenomenon of surface acoustic wave force and heat expansion force. We illustrated successful pumping within a microchannel with surface acoustic wave devices located outside the microchannel patterned on a piezoelectric substrate. Significant advantages of this device are protection of the liquid within the channel, easy and low cost fabrication, no contact between the pumping device and the liquid, homogenous steady laminar flow and small-scale precise liquid control and delivery. Due to the large friction force of the microchannel walls surrounding the liquid, a hydrophobic surface coating (Cytos) was investigated in detail and increased pumping velocity was demonstrated. Our studies indicate that the pumping velocity for a constant liquid volume with the same applied input power can be increased by over 130 % (2.31 vs 0.99 mm/min) by employing a hydrophobic surface coating (Cytos) in a thinner microchannel (250 vs 500 μm) design. This microchannel pump can be used as circulation, dosing, metering and drug delivery applications in which small-scale precise liquid control and delivery is important.

References

- Alghane M et al (2011) Streaming phenomenon induced by Rayleigh surface acoustic wave in microdroplets. *J Appl Phys* 109:0–12
- Alghane M et al (2012) Frequency effect on streaming phenomenon induced by Rayleigh surface acoustic wave in microdroplets. *J Appl Phys* 112:084902
- Cecchini M, Girardo S, Pisignano D, Cingolani R, Beltram F (2008) Acoustic-counterflow microfluidics by surface acoustic waves. *Appl Phys Lett* 92:104103
- Cordeiro AL et al (2009) Fluorination of poly(dimethylsiloxane) surfaces by low pressure CF₄ plasma—physicochemical and anti-fouling properties. *Express Polym Lett* 3:70–83
- Dung Luong T, Trung Nguyen N (2010) Surface acoustic wave driven microfluidics—a review. *Micro Nanosyst* 2:217–225
- Feder ME *Environmental Physiology of the Amphibians*. (University of Chicago Press, 1992). <https://books.google.com/books?hl=en&lr=&id=oaS-OpEjPtUC&pgis=1>. Accessed 1 Nov 2015
- Girardo S, Cecchini M, Beltram F, Cingolani R, Pisignano D (2008) Polydimethylsiloxane–LiNbO₃ surface acoustic wave micro-pump devices for fluid control into microchannels. *Lab Chip* 8:1557
- Guldiken R, Jo MC, Gallant ND, Demirci U, Zhe J (2012a) Sheathless size-based acoustic particle separation. *Sensors* 12:905–922
- Guldiken R, Jo MC, Gallant ND, Demirci U, Zhe J (2012b) Sheathless size-based acoustic particle separation. *Sensors (Basel)* 12:905–922
- Jo MC, Guldiken R (2012) Active density-based separation using standing surface acoustic waves. *Sens Actuators A Phys* 187:22–28
- Jo MC, Guldiken R (2013) Dual surface acoustic wave-based active mixing in a microfluidic channel. *Sens Actuators A Phys* 196:1–7
- Jo MC, Guldiken R (2014a) Particle manipulation by phase-shifting of surface acoustic waves. *Sens Actuators A Phys* 207:39–42
- Jo MC, Guldiken R (2014b) Effects of polydimethylsiloxane (PDMS) microchannels on surface acoustic wave-based microfluidic devices. *Microelectron Eng* 113:98–104
- Kaletta UC, Wenger C (2014) FEM simulation of Rayleigh waves for CMOS compatible SAW devices based on AlN/SiO₂/Si(100). *Ultrasonics* 54:291–295
- Kockmann N (2006) Micro process engineering. *Fluid Dyn Comput Model Appl*. doi:10.1002/9783527616749
- Laser DJ, Santiago JG (2004) A review of micropumps. *J Micromechanics Microengineering* 14:R35–R64
- Masini L et al (2010) Surface-acoustic-wave counterflow micropumps for on-chip liquid motion control in two-dimensional microchannel arrays. *Lab Chip* 10:1997
- Mata A, Fleischman AJ, Roy S (2005) Characterization of polydimethylsiloxane (PDMS) properties for biomedical micro/nano-systems. *Biomed Microdevices* 7:281–293
- Mohanan A, Islam M, Ali S, Parthiban R, Ramakrishnan N (2013) Investigation into mass loading sensitivity of sezawa wave mode-based surface acoustic wave sensors. *Sensors* 13:2164–2175
- Murochi N, Sugimoto M, Matsui Y, Kondoh J (2007) Deposition of thin film using a surface acoustic wave device. *Jpn J Appl Phys* 46:4754–4759
- Rahimi P, Ward C (2005) Kinetics of evaporation: Statistical rate theory approach. *Int J Thermodyn* 8:1–14
- Schmid L, Wixforth A, Weitz DA, Franke T (2012) Novel surface acoustic wave (SAW)-driven closed PDMS flow chamber Microfluid. *Nanofluidics* 12:229–235
- Shabani R, Cho HJ (2011) Active surface tension driven micropump using droplet/meniscus pressure gradient. 2011 16th International Solid-State Sensors, Actuators Microsystems Conference TRANSDUCERS'11 180:1296–1299
- Sritharan K, Strobl CJ, Schneider MF, Wixforth A, Guttenberg Z (2006) Acoustic mixing at low Reynold's numbers. *Appl Phys Lett* 88:054102
- Tan MK, Yeo LY, Friend JR (2009) Rapid fluid flow and mixing induced in microchannels using surface acoustic waves. *EPL Europhys Lett* 87:47003
- Tseng W-K, Lin J-L, Sung W-C, Chen S-H, Lee G-B (2006) Active micro-mixers using surface acoustic waves on Y-cut 128° LiNbO₃. *J Micromechanics Microengineering* 16:539–548
- Uchida D et al. (2003) PDMS Microfluidic devices with PTFE passivated channels. 7th International Conference Miniaturized. *Chem Biochem Anal Syst* 429–432